

Journal of Materials and Engineering Structures

Research Paper

A Numerical Simulation Approach for Investigation of the Pressure Coefficient on the Main Building at the Hill's Top Under the Interference.

Kamlesh A. Mehta [a],*, Jigar K. Sevalia [b]

[a] *Research Scholar, Civil Engineering Department, Gujarat Technological University, Ahmedabad, India*

[b] *Faculty of Civil Engineering, Sarvajanik College of Engineering & Technology, Surat, India*

ARTICLE INFO

Article history:

Received : 8 March 2022

Revised : 1 April 2023

Accepted : 24 April 2023

Keywords:

Computational Fluid Dynamic

Tall Building

3 – Dimensional Hill

Pressure Coefficient

ABSTRACT

The majority of the time, existing codes and standards are used to predict wind loads on structures. The criteria of these standards are based on a wind tunnel test that was done on a single building. On the other hand, buildings rarely stand alone. Wind loads on the principal building are increased or decreased as a result of interference effects caused by interfering buildings. A numerical simulation using ANSYS Fluent 2020 R1 is used in this research to investigate the impact on wind pressure on main building under the interference condition on the hill's top. The external average pressure coefficient on main building on hill's top are determined in the presence of interfering building with varying height ratios of 0.5, 0.75, 1.0, and 1.25, and spacing to width ratios of 0.5, 1.0, 1.5, and 2.0 on 3-D hill. The pressure coefficient decreases as the height of the interfering building rises, showing an increase in the shielding effects of the structure in the vicinity. Nevertheless, when the height of the interfering building is 0.5 of the height of the main building, it is found that the shielding effect has a significant impact on the main building. Because of its placement at the top of the hill, found a significant difference in the pressure coefficient on the rear face of the main building.

1 Introduction

Growing populations, land scarcity, and therefore increasing land costs, particularly in urban regions, demand the construction of taller structures. People are moving from urban areas to rural areas as a result of population expansion and land scarcity in metropolitan areas. Tall buildings on flat terrain are suitable in rural areas where the wind profile has been well established and the behaviour of structures under wind excitation has been thoroughly studied. The development of more complex terrain areas, such as those with hills or undulating terrain, would be required as this region became less appropriate for agricultural use. The fact that hills cannot be utilised for agriculture means that their influence on existing structures may

* *Corresponding author. Tel.: +0919737752301.*
E-mail address: mehta_kamlesh1@gtu.edu.in

e-ISSN: 2170-127X, (cc) BY-SA

RESEARCH REVIEW of Sciences and Technologies

be advantageous. Tall structures, on the other hand, are unusual in urban areas, where they are usually seen as part of a tall structure. In hilly areas, a similar situation may arise in the not too near future. It is important to note that the wind force acting on tall principal buildings is much different than the wind force acting on an isolated building. Interfering structures in close proximity modify the wind flow patterns around main or principal buildings due to elevation of the hill.

As the flow speed increases near the top of the hill, tall structures are subjected to increased or decreased wind pressure, which may lead to structural damage. Changing wind patterns around tall buildings or structures may cause serious environmental issues at the top of a hill. On top of the hill, lateral pressures, especially wind loads, must be considered while constructing tall structures. Possible problems on the hills' leeward slopes may arise from flow separation and recirculation. Having a better understanding of the effects and difficulties of hill influence is essential to make better decisions. Interference mechanisms are influenced by hill shape and size, topographical changes, the size and shape of tall buildings, and the proximity of interfering objects to one other. In order to reduce turbulence caused by the interfering building at the top of the hill, the best distance between the interfering and principal tall structures is being investigated in detail. On top of the hill, the interfering and principal buildings of the symmetrical bluff bodies have the same square cross-section. Computational Fluid Dynamics (CFD) is used to calculate the wind flow around a row of two buildings at wind incidence angle of 0°. Two and three tall structures of the same height might interfere with each other, according to Xie and Gu [1]. Increasing the width of interfering structures enhances the shielding effect and reduces the interference factor (IF). Because of this, two neighbouring interfering structures may have a considerable impact on the principal building's mean wind load. Blocken et al. [2] used CFD and wind tunnel experiments to investigate the venture-effects on the rise of wind speed in pedestrian passages and found that the flow rate through the channel is nearly 8% greater than the free-field flow rate. Mendis et al. [3] present an overview of advanced wind design and explain the outstanding advantages that they provide over basic techniques, as well as emphasise interference from other structures, wind directionality, and cross wind response, which are all key elements in the wind design of tall buildings. Braun and Awruch [4] attempted to provide broad guidelines for aerodynamic and aeroelastic analyses using a common tall building model developed by the CAARC (Commonwealth Advisory Aeronautical Council). The building's surface was surveyed for pressure and aerodynamic coefficients. It was a good fit when the results were aligned with other experimental and numerical predictions. There were considerations for minimal turbulence or flow conditions. It has been widely utilised to evaluate wind loads on tall structures using wind tunnel studies and to validate experimental techniques using CFD, as shown by Agerneh et al. [5]. Wind tunnel data from the laboratory is used to compare numerically calculated pressure coefficients on the surface of the CAARC building under various building configurations. Lam et al. [6] found negative pressure and single-wake flow behaviour in interference effects between two closely spaced tall buildings. The research also evaluated the across-wind load. The load spectra load fluctuations are significantly less than the isolated building situation. Kim et al. [7] calculated wind pressure coefficients and compared them to those of an isolated building, as well as determining the interference effects of the least pressure coefficient at various wind angles. Bairagi and Dalui [8, 9] investigated the appropriate distance between a primary building and an interfering building at which the interference effect does not have an impact on the principle building for wind incidence angles between 0° and 90° degrees. Kheyari and Dalui [10] studied the interference effect that might occur between two structures that are at different altitudes and distances from one another. The analytical technique was used by Jana et al. [11] to determine the IF of a pentagonal plan shape tall structure when wind flow was impeded by two square plan shape tall buildings. Kar and Dalui [12] calculated the IF of an octagonal tall structure that was surrounded by tall buildings with a square plan shape and showed the IF contour. Roy and Bairagi [13] provided the pressure and force coefficients of unconventional tall buildings with a variety of geometrical shapes and configurations. On a 'N'-shaped tall structure, Mukherjee and Bairagi [14] determined the pressure and force coefficients, in addition to the turbulence pattern around the building. Bairagi and Dalui [15, 16] used their power spectral density function to demonstrate the aerodynamic impacts of setback tall buildings on setback tall buildings. Interfering buildings with breadth ratios of 0.4, 0.6, 0.8, 1.0, 1.2, and1.4 were studied by Yu et al. [18], For breath ration, the envelop interference factor was in the range of 0.40 to 0.60. EIFs of 2.3 and 2.1 were the highest along-wind values. Computational Fluid Dynamics (CFD) is used in this investigation, where two bluff bodies are placed inside the domain. It is noticed that the wind pressure and interference factor (*IF*) on the major building are affected by various wind conditions and orientations of the interfering model. Amin and Ahuja [18, 19] used a wind tunnel test to study the mean interference effects between two rectangular buildings in close vicinity in a geometrical configuration of “L” and “T” plan shape, as well as the impact of wind direction and position of upstream building in influencing the responses of tall structures.

Tall structures are routinely subjected to wind tunnel experiments to assess wind loads and interfering phenomena. It gives a more precise evaluation of wind flow around a tall structure, but it is time-consuming and cost wise very expensive. CFD, on the other hand, allows greater flexibility in conducting parametric analyses for various wind flow conditions,

geometries, and complex surroundings at a reduced cost. While the phenomena have been researched, there is no research work on the impacts of the interfering building's height on the principal building on the top of the hill or complex terrain.

2 Description of Simulation

2.1 Model of the Tall Building on the Hill's Top in details

A square prism with full-size dimensions of H = 85 m, L = 30 m, and B = 30 m was selected for this study of tall building under the interference condition. This tall building on top of the hill is situated within a rectangular domain with varying dimensions. These two models of square-plan buildings with aspect ratios of 0.5, 0.75, 1.0, and 1.25 were evaluated in this research study, one of which is the interfering building (M – 1) and the other is the principal building (M – 2). In this investigation, the theory of Computational Fluid Dynamics (CFD) is used to analyse the wind loads of the principal building for spacing to width ratios (*S/B*) ranging from 0.5 to 2.0 of the two buildings for wind incidence angles for 0° on 85 m hill height as listed in Table1.

Table 1 – Details of Interference Building (M – 1) and Principal Building (M – 2) with Dimension.

Plan Dimensions of both tall Building (m^2)	Height of Hill (H_h) (m)	Height of Principal Building (M – 2) (H) (m)	Height to Height Ratio (h/H)	Height of Interfering Building (M – 1) (h) (m)
30 × 30	85	85	0.50	42.50
30 × 30	85	85	0.75	63.75
30 × 30	85	85	1.00	85.00
30 × 30	85	85	1.25	106.25

2.2 Configuration of Hill

Based on an equation (1) including the cosine square functions [20, 21] and the topography factor (k3) given by the Indian Standards of practice IS: 875 (Part-3), 2015. A basic axisymmetric 3 – dimensional hill model is developed as shown in figure 1(c).

$$z_{x,y} = H_h \cos^2\left[\pi \frac{\sqrt{x^2+y^2}}{2L_e}\right] \tag{1}$$

"x" denotes a dimension parallel to the wind direction, "y" denotes the lateral side perpendicular to "x", and "z" denotes a dimension perpendicular to both "x" and "y." The hill's features include its height ("H_h") of 85 metres, its effective length ("L_e") of 180 metres, its base radius ("L") of 310 metres, and its upward slope ("s") of 18°.

2.3 Details of Domain and Meshing

The research domain should be large enough to prevent fluid streams from reflecting and creating an unsuitable pressure field around the building models on hill's top. The domain size in this study is chosen by Franke et al. [22] and Revuz et al. [23]. As shown in figure 1(a) and 1(b), the domain has a 5H upstream fetch, 15H downstream fetch, and 5H side and top clearance from top of the tall building with 3 – dimensional geometry of the domain with building's orientation as shown in figure 1(d). Using hexahedral structured meshing using for the numerical simulation as shown in figure 2 under the isolated tall building for the checking purpose of reliability of the CFD as well as for the interference condition on hill's top. Wind direction facing walls of domain and the top of the boundary are referred to as "FREE SLIP WALLS"; all other walls, 3-dimensional hill are referred to as "NO-SLIP WALLS."

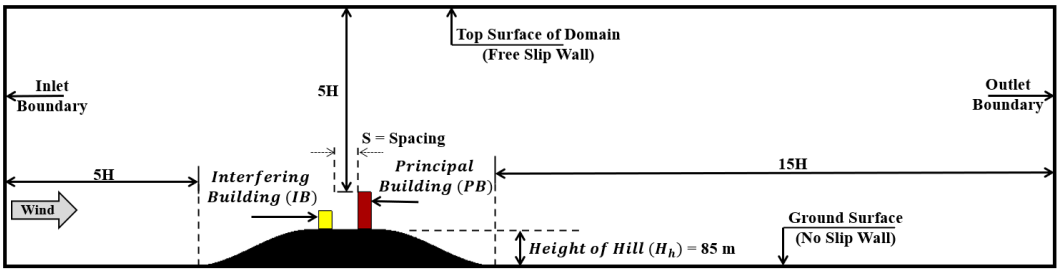

(a) Side Elevation of Domain

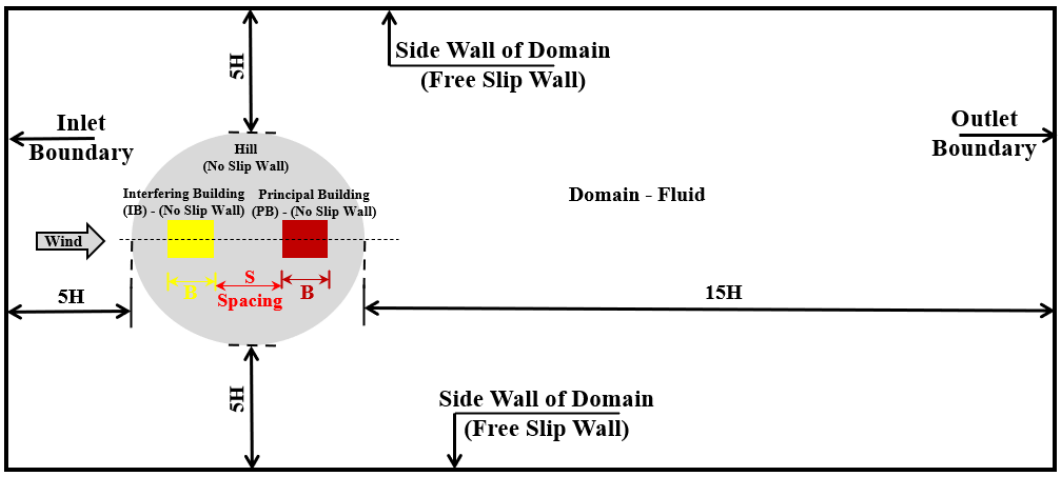

(b) Top View of Domain

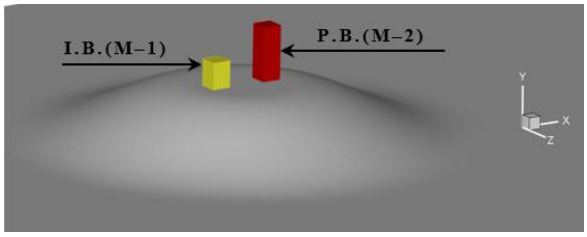

(c) 3 – Dimensional Geometry

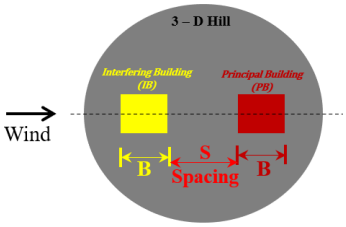

(d) Building Orientation

Fig. 1 – Details of Building Models (B.M.) in Fluid Domain with Orientation.

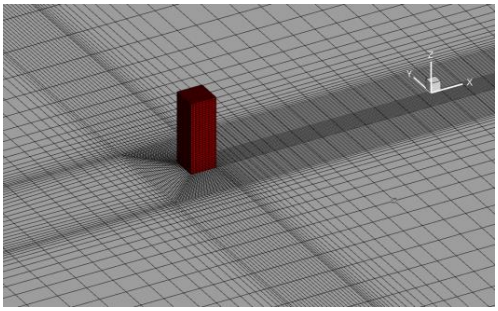

(a) Isolated Condition on flat surface

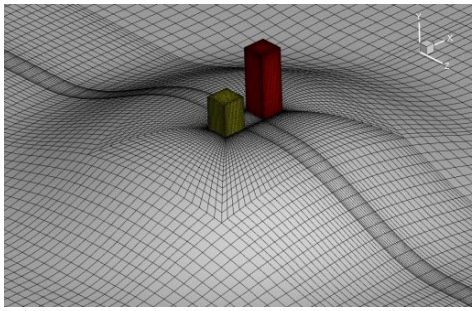

(b) Interference Condition on Top of Hill

Fig. 2 – Hexahedral Structured Meshing

2.4 Wind Profile Simulations

Jackson and Hunt [24] categorised hill height and shape in their model for flow over hills. The effects of wind moving over hills are fairly constant. The change in wind profile at the top of the hill is shown in figure 3, but an explanation of the impacts is important. There is a minor slowing near the surface at the foot of the upwind side of the slope. This deceleration may generate a little separation bubble if the gradient is steep enough. The flow accelerates up to the top of the hill, where it reaches its maximum velocity. The flow then slowed as its foot of the leeward side of the slope. Pressure and velocity contour diagrams generated by the ANSYS Fluent 2020 R1 are shown in the figure 4.

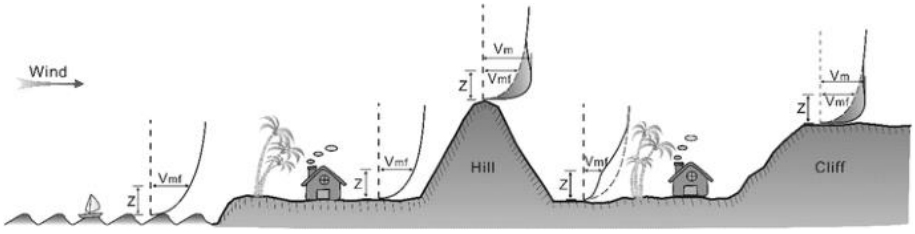

Fig. 3 – Variations in wind profile due to topographic influences are depicted in this diagram

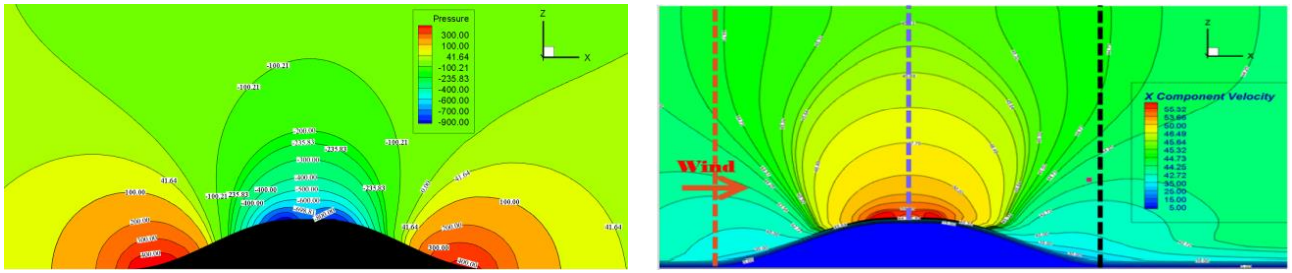

Fig. 4 – Pressure and Velocity Contour – Vertical Centre Plane

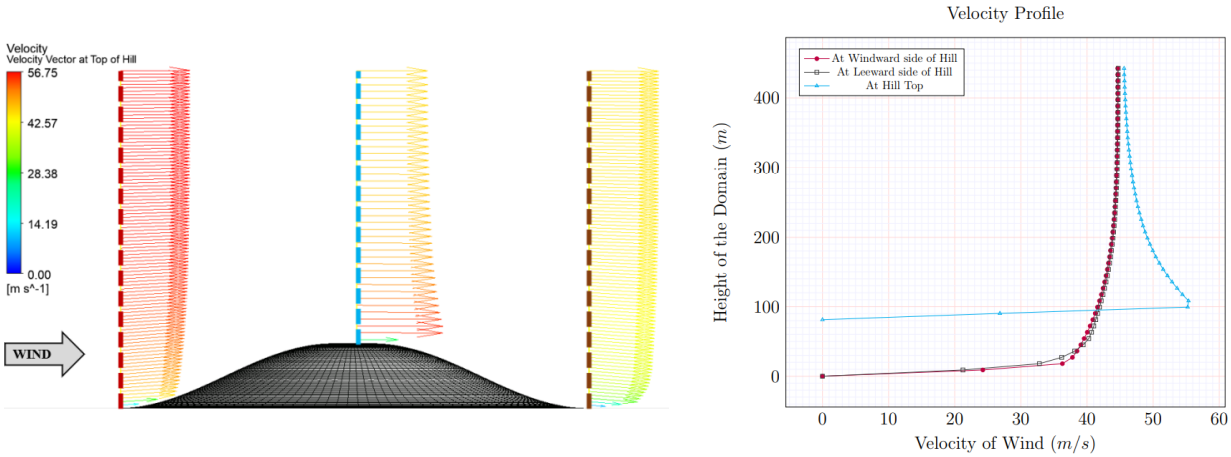

Fig. 5 – Velocity Profile at Different Location

The power law or logarithmic law may both be used to describe the velocity profile. When it comes to civil engineering applications, power law is frequently utilized. In this work, a wind velocity profile with a power law exponent of 0.14 is simulated that is close to terrain category-II as specified in IS: 875 (Part-3), 2015 [21] and has a terrain category-II terrain category. According to the power law, wind velocity is defined as follows

$$U_{(z)} = U_0 \left(\frac{z}{z_0}\right)^{\propto} \tag{2}$$

where, "U_0" is the basic wind speed, which is taken as 44 m/s. The wind pressures on the principal building under isolated and interfering conditions are examined using the computational fluid dynamic software ANSYS Fluent 2020 R1in this study. Figure 5 shows that the wind velocity at the Earth's surface is very close to zero up to a certain height and then rises with height, which may be described as a power law. The variance in mean wind speed is greatly influenced by the different kinds of terrain. Complex terrain affects the near-surface wind speed, pressure and turbulence pattern. There seems to be a having an increase in wind speed.

2.5 Governing equations

Today, there are a variety of numerical simulation approaches available to researchers. Because of their high computational costs and difficulties in modification, Large-eddy simulation (LES) and Direct Numerical Simulation (DNS) are only rarely employed for rural wind calculations and wind studies [25, 26], respectively. Furthermore, [26] said that LES is suitable for wind flow computation, while [27] and [28] stated that simulations from a variety of wind directions are often done for pedestrian-level wind flow study [27]. This has resulted in the use of RANS stable analysis for wind flow computation [25] and [26] because to the high processing cost of transient analysis. In our previous study [29], we analysed that compared to k – ω (SST) method, k – ε (Realizable) turbulence method provide better results for prismatic shapes. As a result of this quick review, the traditional k (Realizable) turbulence model was selected for use in this investigation [30] developed the current "SKE turbulence model," which is a variation of the standard k (Realizable) turbulence model. [31] contains the model transport equations for the variables k and. The governing equations are shown in the following equation

$$\frac{\partial}{\partial t}(\rho k) + \frac{\partial}{\partial x_j}(\rho k u_j) = \frac{\partial}{\partial x_i}\left[\left(\mu + \frac{\mu_t}{\sigma_k}\right)\frac{\partial k}{\partial x_j}\right] + G_k + G_b - \rho\varepsilon - Y_M + S_k \tag{3}$$

$$\frac{\partial}{\partial t}(\rho \varepsilon) + \frac{\partial}{\partial x_j}(\rho \varepsilon u_j) = \frac{\partial}{\partial x_j}\left[\left(\mu + \frac{\mu_t}{\sigma_\varepsilon}\right)\frac{\partial \varepsilon}{\partial x_j}\right] + \rho C_1 S\varepsilon - \rho C_2 \frac{\varepsilon^2}{k+\sqrt{v\varepsilon}} + C_{1\varepsilon}\frac{\varepsilon}{k}C_{3\varepsilon}G_b + S_\varepsilon \tag{4}$$

where,

$$\boldsymbol{C_1 = max\left[0.43, \frac{n}{n+5}\right], n = S\frac{k}{\varepsilon}, S = \sqrt{2S_{ij}S_{ij}}}$$

Turbulence kinetic energy is called G_k because of the mean velocity gradients, G_b because of buoyancy, and Y_M because of the fluctuating dilation in compressible turbulence. C_1 and C_2 are the constants. σ_k & σ_ε represents the turbulent Prandtl number for kinetic energy, which is called k and ε is also called as dissipation rate. All of the other symbols have the same meaning they always have. FLUENT specified the constants are $C_{2\varepsilon}$= 1.9, σ_k= 1 and σ_ε =1.2. The building was thought of as a bluff body, and the flow around it was looked at. Air has a density of considered as 1.224 kg/m^3. There was a speed of 44 m/s inlet and a pressure of zero Pa at the outlet of the domain. Turbulence intensity was thought to be 0.10%.

2.5.1 Solver Settings

The results were all steady-state in nature. For the pressure, momentum, and turbulence equations, second-order differencing was utilised, as well as the "coupled" pressure-velocity coupling method, which is more durable for steady-state, single-phase flow problems. After many hundred repetitions, the residuals fell below the generally used criterion of falling to 10^{-4} of their initial values. The average pressure value acting on the tall building, was measured during the simulation, and only when they achieved stable and constant values were the simulations considered to have converged. Despite the fact that the simulations were steady-state, the "steady" values of the different monitoring data varied by about 1%.

3 Analysing the findings of a square model to measure the software's reliability:

When the wind angle is 0°, the contours of the pressure distribution on different faces correspond to the isolated condition of a square-shaped building model having size 30 x 30 x 90m on a flat horizontal ground as shown in figure 6. The distribution of pressure is symmetrical about the vertical centreline at the central front face and back face of isolated building, i.e. at the front face and the back face, respectively. As predicted, pressure on the whole front face is higher and more positive than on the back face. The high-pressure region is located on the central upper surface, while the lower pressure region is located on the bottom of the side edges, and the narrow band of strong negative pressure towards the front face develops because of the

front face's separation of the wind flow. Suction is experienced on the back face, with an equally even distribution across the horizontal axis. Because of the symmetry of wind flow, the pressure distribution on all the side surfaces and back face is under suction as expected due to side wash and vortices generated in the wake. As shown in Table 2, the estimated pressure coefficients using ANSYS Fluent 2020 R1 are almost identical to experimental values from Amin and Ahuja [32], IS: 875 (Part-3) 2015 [21], ASCE-7 [33], and AS/NZS 1170-02 [34]. Due to the creation of unstable vortices in the wake areas near the back face, there may be a little disparity in pressure coefficients on the back face.

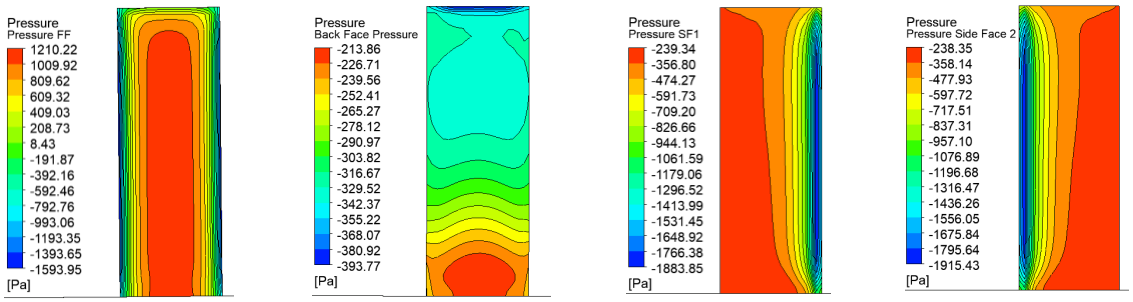

(a) Front Face ***(b) Back Face*** ***(c) Side Face – 1*** ***(d) Side Face – 2***

Fig. 6 – Pressure contours on different faces of square model for normal wind angle – (0°)

Table 2 – Comparison of Wind Pressure Coefficient on Principal Building in Isolated Condition.

Faces	Front Face	Back Face	Side Wall - 1	Side Wall - 2
ANSYS Fluent	0.84	-0.50	-0.67	-0.67
IS: 875 (Part-3), 2015 [21]	0.80	-0.25	-0.80	-0.80
Amin and Ahuja [32]	0.74	-0.50	-0.69	-0.69
ASCE 7-10 [33]	0.80	-0.50	-0.70	-0.70
AS/NZS1170-2 (2002) [34]	0.80	-0.50	-0.65	-0.65

4 Results and Discussions of Interference Effects

In reality, the flow pattern on the hill's top is determined by two pressure systems around the principal building (M – 2). The first pressure system generated between the two buildings, with maximum pressure at the stagnation point and decreased pressures throughout the front face. This pressure system is formed when the approach flow wind speed increases with height, and it is responsible for the formation of the standing vortex, which feeds the corner streams. The under-pressure zone on the building's leeward side or back face constitutes the second pressure system. It is in responsible of the recirculation (backflow) of wind downstream of the building, as well as the corner streams and recirculation of wind around the hill. The complex wind flow pattern that exists around the main building (M – 2) on the hilltop is caused by both pressure systems.

Specifically, two building models, an interfering building (M – 1) and a principal building (M – 2), are placed in tandem positioned on an 85-meter hilltop with varying h/H ratios of 0.5, 0.75, 1.0, and 1.25 and with varying spacing-to-width ratio of 0.5, 1.0, 1.5, and 2.0 are considered, and the pressure distribution on the principal building (M – 2) is observed and analysed.

4.1 Case – I: Pressure coefficient on Principal Building (M – 2) under the Interference Condition for h/H ratio = 0.5

The figure 7 shows the wind flow patterns between (M – 1) and (M – 2), that are placed in tandem positioned at various spacing to width ratio (*S/W*) 0.50, 1.00, 1.50, and 2.00 from one other for the height of interfering building = 0.5. At close range (*S/B* = 0.50), the interfering building's (M – 1) obstruction effect is obvious, and no cohesive vortex forms between the two buildings. Increasing the spacing to width ratio (*S/B* ratio 0.50 to 2.0) creates a large vortex that is aided by the shear flow separation created by the interfering building (M – 1), lowering the wind flow to the ground. The enormous, stable vortex is replaced by the wake turbulence that separates from the interfering building (M – 1) as the distance increases. As the distance increases, the interfering building's (M – 1) effect reduces.

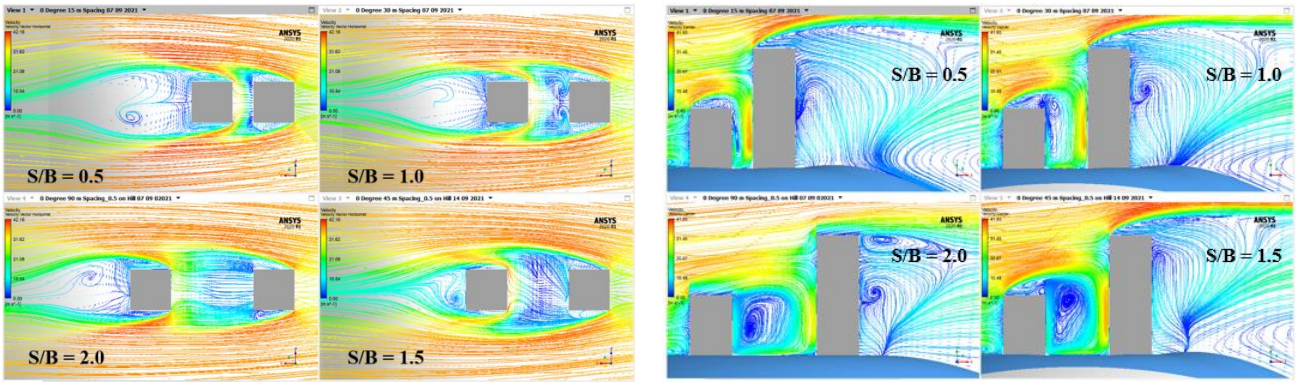

Fig. 7 – Wind Flow Patterns (Horizontal and Vertical) for Various S/B ratio with h/H Ratio – 0.5

The figure 8 illustrates that, as the spacing to width ratio reduces, pressure rises; that is, when two buildings are tandem in positioned, the pressure increases to its maximum observed at stagnation point about 0.8*H* to 0.85*H* level from hill's top. From stagnation point, the flow is deviated to the lower pressure zones of the facade: upwards, sidewards, and downwards. The considerable amount of air flowing downwards produces vortices at the 0.25*H* to 0.5*H* from the ground level of hill's top by the shear flow separation created by the interfering building (M – 1).

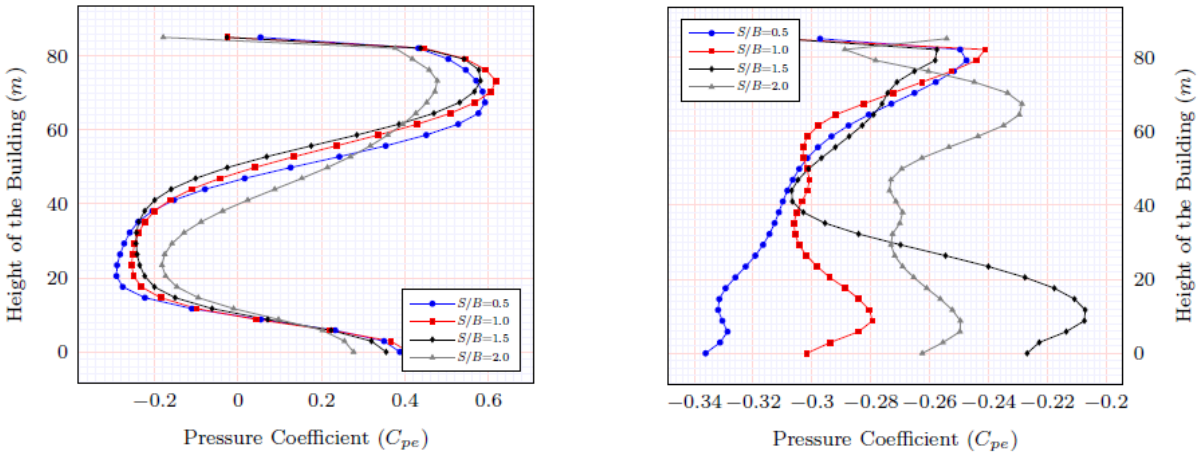

(a) Front Face ***(b) Back Face***

Fig. 8 – Pressure Coefficient on centre (M – 2) for Various S/B ratio with h/H Ratio – 0.5

According to figure 8, A low-pressure zone is formed on the leeward side of the principal building's (M – 2), because of backflow or recirculation from slope and shear flow separation from lateral sides of the principal building (M – 2) at wake region of the principal building (M – 2) and creates the slow-moving vortices and found low speed at leeward side of principal building (M – 2). As a result, increase in pressure with lower spacing to width ratio = 0.5 when decreases the pressure value with increase with spacing to width ratio from 0.5 to 2.0 and slow at near ground level.

4.2 Case – II: Pressure coefficient on Principal Building (M – 2) under the Interference Condition for h/H ratio = 0.75

There are four different spacing to width ratios illustrated in this diagram for a height-to-height (*h/H*) ratio of 0.75, each representing a different height to height (*h/H*) ratio of the interfering building (M – 1) and the principal building (M – 2) when they are placed in tandem. *S/B* = 0.50, the intervening building's obstruction effect is naturally obvious, and a cohesive vortex emerges between the two buildings. As seen in the figure 9, interfering building (M – 1) induces shear flow separation from the top surface, which causes a low-pressure zone in between two buildings. By increasing the spacing to width ratio from 0.50 to 2.0, enormous vortices are generated. Large, stable vortices are formed when there is an increase in distance between principal building (M – 2) and an interfering building (M – 1), which is caused by *h/H* ratio of the interfering building (M – 1) wake region.

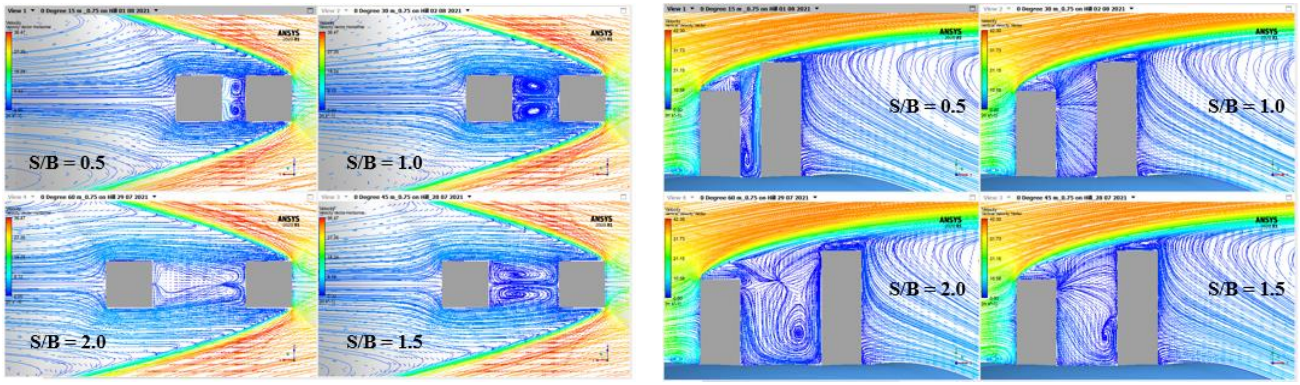

Fig. 9 – Wind Flow Patterns (Horizontal and Vertical) for Various S/B ratio with h/H Ratio – 0.75

The existence of the upstream interference building in tandem causes negative pressure on the windward face of the principal building (M – 2). Compared to a similar structure in an isolated situation, the leeward face of the principal building (M – 2) is exposed to less pressure because of an upstream interfering building (M – 1) with a *h/H* ratio of 0.75. In general, the shielding generated by the interfering building (M – 1) for *h/H* ratio of 0.75 is much greater than the shielding produced by the interfering building (M – 1) with a *h/H* ratio of 0.5 as shown in figure 10.

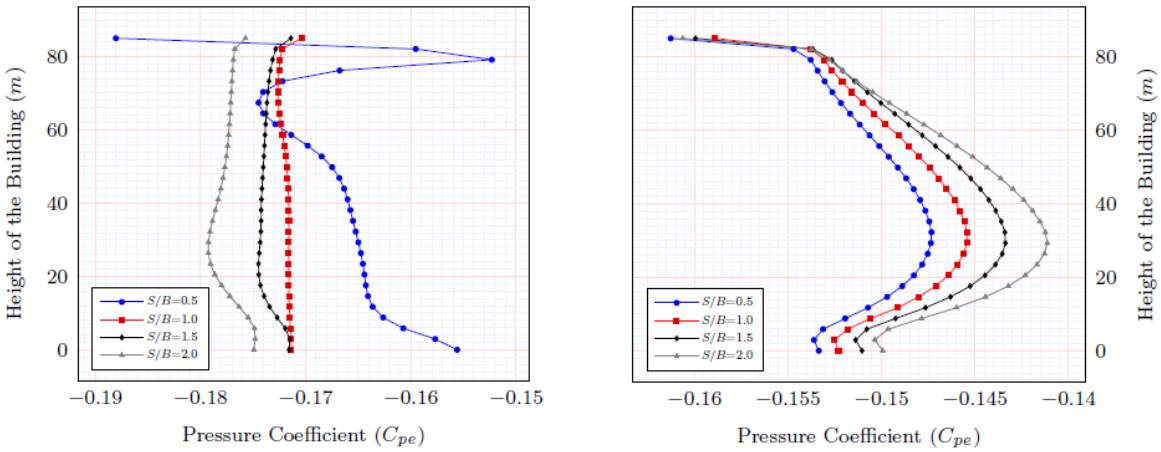

(a) Front Face ***(b) Back Face***

Fig. 10 – Pressure Coefficient on centre of (M – 2) for Various S/B ratio with h/H Ratio – 0.75

The figure 10 illustrates that, as the spacing to width ratio increases from 0.5 to 2.0, pressure decreases; that is, when two buildings are tandem in positioned, the pressure decreases to its minimum observed at stagnation zone about 0.35*H* to 0.4*H* level and it is marked where the flow directions are opposite and low wind speeds are found on the leeward side of the principal building (M – 2) on hill top. At stagnation zone, the flow is deviated to the upwards, sidewards, and downwards.

4.3 Case – III: Pressure coefficient on Principal Building (M – 2) under the Interference Condition for h/H ratio = 1.0

In this case, four different spacing to width ratios illustrated in this diagram for a height to height (*h/H*) ratio of 1.00, each representing a different height to height (*h/H*) ratio of the interfering building (M – 1) and the principal building (M – 2) when they are placed in tandem. *S/B* = 0.50, the intervening building's obstruction effect is naturally obvious, and a cohesive vortex emerges between the two buildings. As seen in the figure 11, interfering building (M – 1) induces shear flow separation from the top surface, which causes a low-pressure zone in between two buildings. By increasing the spacing to width ratio from 0.75 to 2.0, enormous vortices are generated. Large, stable vortices are formed when there is an increase in distance between principal building (M – 2) and an interfering building (M – 1), which is caused by *h/H* ratio of the interfering building (M – 1) wake region.

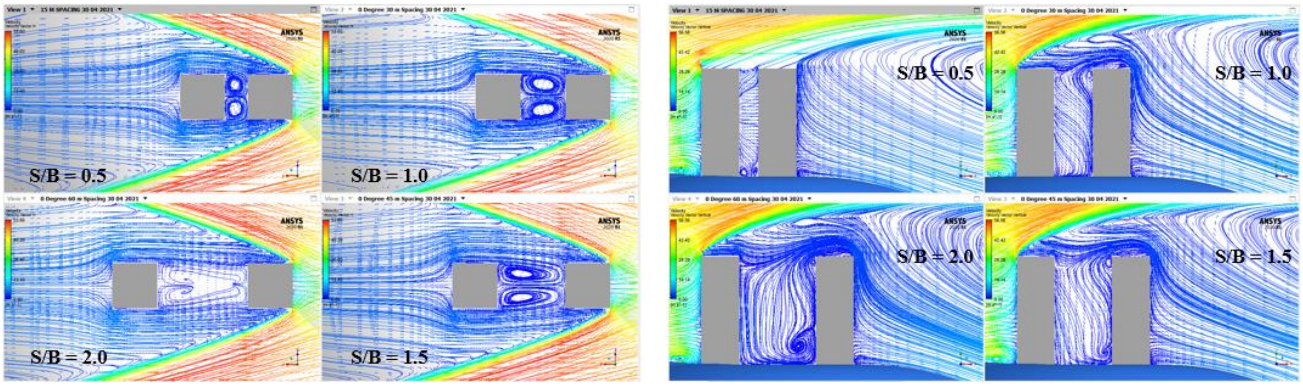

Fig. 11 – Wind Flow Patterns (Horizontal and Vertical) for Various S/B ratio with h/H Ratio – 1.0

In this case, the negative pressure coefficient is generated to the windward face of the principal building (M – 2) due to the presence of the interfering building (M – 1) in the front region. When compared to pressures on similar buildings in with h/H ratio 0.75, the magnitude and distribution of pressures on the windward and side faces of the principal building (M – 2) vary significantly in the presence of interference buildings (M – 1) at various spacing to width ratio on the windward and side faces of the principal building (M – 2) as shown in figure 12.

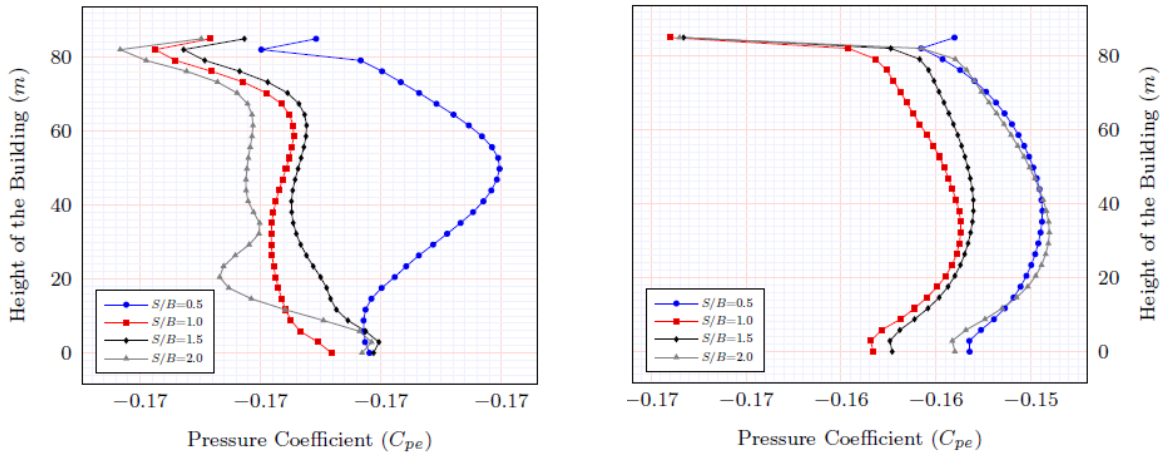

(a) Front Face ***(b) Back Face***

Fig. 12 – Pressure Coefficient on centre of (M – 2) for Various S/B ratio with h/H Ratio – 1.0

When both buildings are in tandem arrangement, it is evident that the mean along-wind force on the downstream principal building (M – 2) is lowered as a result of the presence of the upstream interference building with a h/H ratio of 1.0. When two buildings are in close proximity to one another, a large degree of shielding or a decrease in drag force on the principal building (M – 2) may be seen to occur.

4.4 Case – VI: Pressure coefficient on Principal Building (M – 2) under the Interference Condition for h/H ratio = 1.25

Negative pressure is exerted on the windward face of the principal building as a result of the existence of an interfering building with a height ratio of 1.25 that is located directly in front of the principal building and has a spacing to width ratio of 0.5 to 2.0 that is in tandem arrangement.

In this case, four different spacing to width ratios illustrated in this diagram for a height to height (*h/H*) ratio of 1.25, each representing a different height to height (*h/H*) ratio of the interfering building (M – 1) and the principal building (M – 2) when they are placed in tandem. *S/B* = 0.50, the intervening building's obstruction effect is naturally obvious, and a cohesive vortex emerges between the two buildings. As seen in the figure 13, interfering building (M – 1) induces shear flow separation from the top surface, which causes a low-pressure zone in between two buildings. By increasing the spacing to width ratio from 0.75 to 2.0, enormous vortices are generated. Large, stable vortices are formed when there is an increase in

distance between principal building (M – 2) and an interfering building (M – 1), which is caused by *h/H* ratio of the interfering building (M – 1) wake region as shown in figure 14.

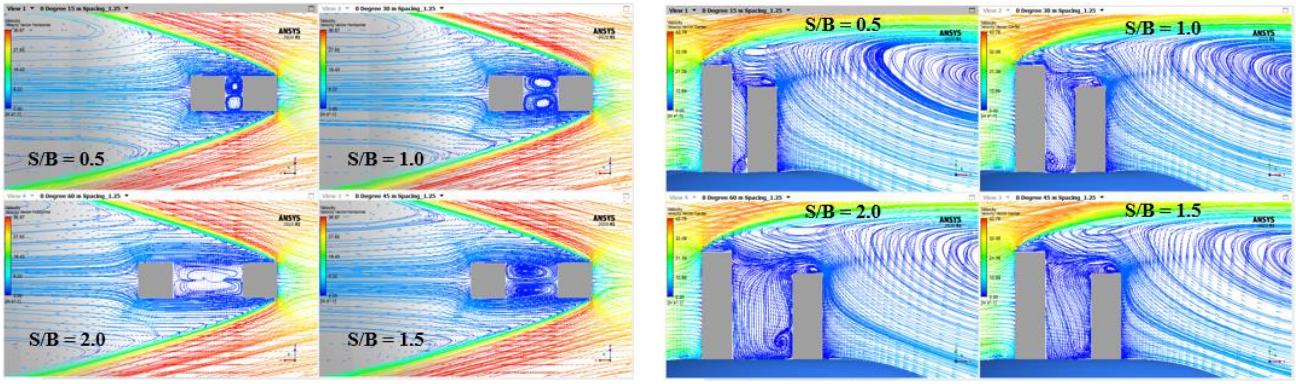

Fig. 13 – Wind Flow Patterns (Horizontal and Vertical) for Various S/B ratio with h/H Ratio – 1.25

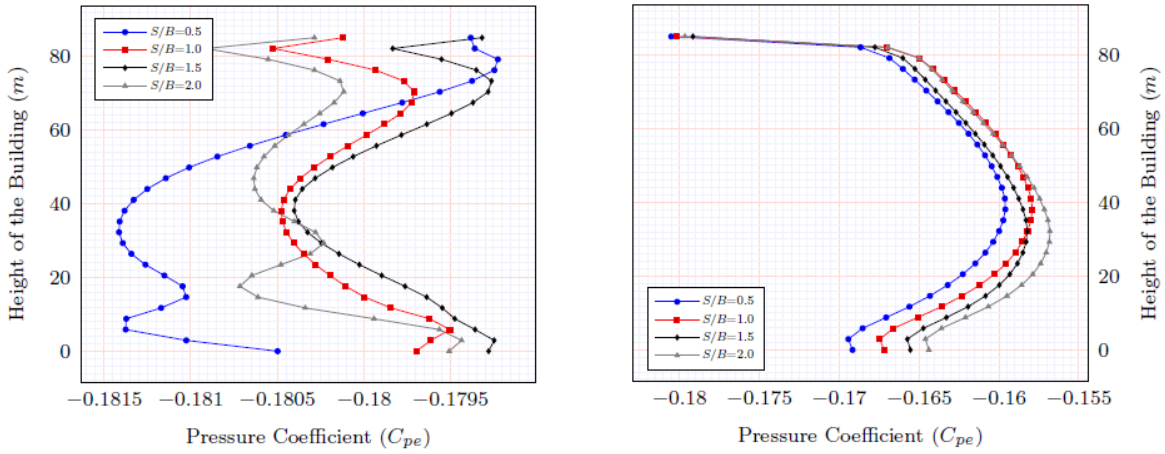

(a) Front Face ***(b) Back Face***

Fig. 14 – Pressure Coefficient on centre of (M – 2) for Various S/B ratio with h/H Ratio – 1.25

5 Conclusions

ANSYS Fluent 2020 R1 software is used to study the mean interference effects between two buildings situated at the top of a hill. The consequences of the height of upstream interference on the principal building are also examined. When the h/H ratio ranges from 075 to 1.25, the effects of the upstream interference building (M – 1) in tandem arrangement are more noticeable, indicating that shielding effects are higher on hill's top. Also, the influence of the h/H ratio of 0.5 is more significant on the pressure coefficient on the front face of the principal building (M – 2) than it is on the back face of the same structure (M – 2).

Because of the height of the interfering building (M – 1), the wind pressure on the principal building (M – 2) might be influenced as well. The interference conditions are very sensitive to the distance between the interfering building (M – 1) and principal building (M – 2) particulars on hill's top. Based on the result, it can be concluded that under the interference from lower interfering buildings (M – 1) with h/H ratio 0.5 is more significant. The interference from the interfering building (M – 1), on the other hand, h/H ratio ranging from 0.75 to 1.25 occurs negative pressure on front face due to interference and on back face due to recirculation of wind flow from the foot of the leeward side of the hill.

REFERENCES

[1]- Z.N. Xie, M. Gu, Mean interference effects among tall buildings. Engineering Structures, 26(9) (2004) 1173-1183. doi:10.1016/j.engstruct.2004.03.007.

[2]- B. Blocken, J. Carmeliet, T. Stathopoulos, CFD evaluation of wind speed conditions in passages between parallel buildings—effect of wall-function roughness modifications for the atmospheric boundary layer flow. Journal of Wind Engineering and Industrial Aerodynamics, 95(9) (2007) 941-962. doi:10.1016/j.jweia.2007.01.013.
[3]- P. Mendis, T. Ngo, N. Haritos, A. Hira, B. Samali, J. Cheung, Wind loading on tall buildings. Electronic Journal of Structural Engineering, 7 (2007) 41-54.
[4]- A.L. Braun, A.M. Awruch, Aerodynamic and aeroelastic analyses on the CAARC standard tall building model using numerical simulation. Computers & Structures, 87(9) (2009) 564-581. doi:10.1016/j.compstruc.2009.02.002.
[5]- A.K. Dagnew, G.T. Bitsuamalk, R. Merrick. Computational evaluation of wind pressures on tall buildings. in 11th Americas Conference on Wind Engineering. San Juan, Puerto Rico. (2009).
[6]- K.M. Lam, M.Y. H. Leung, J.G. Zhao, Interference effects on wind loading of a row of closely spaced tall buildings. Journal of Wind Engineering and Industrial Aerodynamics, 96(5) (2008) 562-583. doi:10.1016/j.jweia.2008.01.010.
[7]- W. Kim, Y. Tamura, A. Yoshida. Interference effects of two buildings on peak wind pressures. in The Seventh Asia-Pacific Conference on Wind Engineering. Taipei, Taiwan. (2009).
[8]- A. Bairagi, S. Dalui. Evaluation of interference effects on parallel high-rise buildings for different orientation using CFD. in 3rd World Conference on Applied Sciences, Engineering & Technology. Kathmandu, Nepal. (2014), 764-774.
[9]- A.K. Bairagi, S.K. Dalui, Optimization of Interference Effects on High-Rise Buildings for Different Wind Angle Using CFD Simulation. Electronic Journal of Structural Engineering, 14 (2014) 39-49. doi:10.56748/ejse.14179.
[10]- P. Kheyari, S.K. Dalui, Estimation of wind load on a tall building under interference effects: a case study. Jordan Journal of Civil Engineering, 9(1) (2015) 84-102.
[11]- D. Jana, T. Bhaduri, S.K. Dalui, Numerical study of optimization of interference effect on pentagonal plan shaped tall building. Asian Journal of Civil Engineering, 16(8) (2015) 1123-1153.
[12]- R. Kar, S.K. Dalui, Wind interference effect on an octagonal plan shaped tall building due to square plan shaped tall buildings. International Journal of Advanced Structural Engineering (IJASE), 8(1) (2016) 73-86. doi:10.1007/s40091-016-0115-z.
[13]- K. Roy, A.K. Bairagi, Wind pressure and velocity around stepped unsymmetrical plan shape tall building using CFD simulation—A case study. Asian Journal of Civil Engineering (BHRC), 17(8) (2016) 1055-1075.
[14]- A. Mukherjee, A. Bairagi, Wind pressure and velocity pattern around ‘N’plan shape tall building—A case study. Asian J. Civil Eng.(BHRC), 18(8) (2017) 1241-1258.
[15]- A.K. Bairagi, S.K. Dalui, Aerodynamic effects on setback tall building using CFD simulation. International Journal of Mechanical and Production Engineering Research and Development, (2018) 413-420.
[16]- A.K. Bairagi, S.K. Dalui, Comparison of aerodynamic coefficients of setback tall buildings due to wind load. Asian Journal of Civil Engineering, 19(2) (2018) 205-221. doi:10.1007/s42107-018-0018-3.
[17]- X. Yu, Z. Xie, M. Gu, Interference effects between two tall buildings with different section sizes on wind-induced acceleration. Journal of Wind Engineering and Industrial Aerodynamics, 182 (2018) 16-26. doi:10.1016/j.jweia.2018.09.012.
[18]- J.A. Amin, A.K. Ahuja, Mean interference effects between two buildings: effects of close proximity. The Structural Design of Tall and Special Buildings, 20(7) (2011) 832-852. doi:10.1002/tal.564.
[19]- J.A. Amin, A. Ahuja, Wind-induced mean interference effects between two closed spaced buildings. KSCE Journal of Civil Engineering, 16(1) (2012) 119-131. doi:10.1007/s12205-012-1163-y.
[20]- S. Yan, S. Shi, X. Chen, X. Wang, L. Mao, X. Liu, Numerical simulations of flow interactions between steep hill terrain and large scale wind turbine. Energy, 151 (2018) 740-747. doi:10.1016/j.energy.2017.12.075.
[21]- IS, 875: Design Loads (Other than Earthquakes) for Buildings and Structures–Code of Practice–Part 3 Wind loads. Bureau of Indian Standards, New Delhi, (2015).
[22]- J. Franke, C. Hirsch, A. Jensen, H. Krüs, M. Schatzmann, P. Westbury, S. Miles, J. Wisse, N. Wright. Recommendations on the use of CFD in predicting pedestrian wind environment. in Cost action C. (2004), 1-12.
[23]- J. Revuz, D. Hargreaves, J. Owen, On the domain size for the steady-state CFD modelling of a tall building. Wind and structures, 15(4) (2012) 313.
[24]- P.S. Jackson, J.C.R. Hunt, Turbulent wind flow over a low hill. Quarterly Journal of the Royal Meteorological Society, 101(430) (1975) 929-955. doi:10.1002/qj.49710143015.
[25]- J. Hang, M. Sandberg, Y. Li, Effect of urban morphology on wind condition in idealized city models. Atmospheric Environment, 43(4) (2009) 869-878. doi:10.1016/j.atmosenv.2008.10.040.

[26]- W.D. Janssen, B. Blocken, T. van Hooff, Pedestrian wind comfort around buildings: Comparison of wind comfort criteria based on whole-flow field data for a complex case study. Building and Environment, 59 (2013) 547-562. doi:10.1016/j.buildenv.2012.10.012.

[27]- A. Avramenko, O. Agafonova, J. Sorvari, H. Haario, Simulation of depth-integrated flow over a hill. AIP Conference Proceedings, 1738(1) (2016). doi:10.1063/1.4952329.

[28]- C. Prigent, I. Tegen, F. Aires, B. Marticorena, M. Zribi, Estimation of the aerodynamic roughness length in arid and semi-arid regions over the globe with the ERS scatterometer. Journal of Geophysical Research: Atmospheres, 110(D9) (2005). doi:10.1029/2004JD005370.

[29]- K. Mehta, J. Sevalia, Effectiveness of CFD simulation of wind flow & its effect on tall structures with aerodynamic shapes. International Journal of Advanced Research in Engineering and Technology (IJARET), 11(12) (2020) 2437-2446.

[30]- D.B. Spalding, The numerical computation of turbulent flow. Comp. Methods Appl. Mech. Eng., 3 (1974) 269.

[31]- I. Ansys, Fluent theory guide, Release 14, 724 – 746 ANSYS Inc, USA, (2013).

[32]- J. Amin, A. Ahuja, Effects of side ratio on wind-induced pressure distribution on rectangular buildings. Journal of Structures, 2013 (2013) 1-12. doi:10.1155/2013/176739.

[33]- ASCE, 7-02 - Minimum design loads for buildings and other structures, Structural Engineering Institute of American Society of Civil Engineers Reston, USA. (2002).

[34]- AS/NZS, Structural design actions, Part-2: Wind Actions. Standards Australia, Sydney, Australia, Standards New Zealand, Wellington, New Zealand, (2002).